Covalent Functionalization of Nanodiamonds by Ruthenium Porphyrin, and Their Catalytic Activity in the Cyclopropanation Reaction of Olefins

Chiara Lorecchio [1], Emanuela Tamburri [1], Laura Lazzarini [2], Silvia Orlanducci [1], Robertino Zanoni [3] and Pietro Tagliatesta [1,*]

[1]   Dipartimento di Scienze e Tecnologie Chimiche, Università di Roma "Tor Vergata",
    Via della Ricerca Scientifica, 00133 Rome, Italy; chiaralorec@hotmail.it (C.L.); tmbmnl00@uniroma2.it (E.T.);
    silvia.orlanducci@uniroma2.it (S.O.)
[2]   IMEM-CNR, Parco Area delle Scienze 37/A, Località Fontanini, 43124 Parma, Italy;
    laura.lazzarini@imem.cnr.it
[3]   Dipartimento di Chimica, Università di Roma "La Sapienza", Piazzale Aldo Moro 5, 00185 Rome, Italy;
    robertino.zanoni@uniroma1.it
[*]   Correspondence: pietro.tagliatesta@uniroma2.it

Abstract: Detonation nanodiamonds (DNDs) were functionalized by ruthenium porphyrins and used as catalysts in the cyclopropanation reaction of olefins. The heterogeneous catalyst was characterized by transmission electron microscopy (TEM), scanning electron microscopy (SEM), and XPS (X-ray photoelectron spectroscopy). The XPS was used to control the binding of the ruthenium porphyrin to the DNDs' surface. This catalyst was used in the cyclopropanation reactions of simple olefins and was reused with no loss of activity in four consecutive cycles, after recovering each time by simple centrifugation.

1. Introduction

The cyclopropyl ring is present in a number of interesting natural products. Recently, this ring has been found in drugs active in vitro against leukemia. [1] Several methods have been proposed in the past for synthesizing this ring, using copper, rhodium and osmium compounds as efficient catalysts for obtaining cyclopropanes from diazocompounds and olefins. [2] Synthetic iron, rhodium and osmium porphyrins have also been reported as catalysts for the cyclopropanation reaction of simple olefins by ethyldiazoacetate (EDA). [3–7] Compared to copper salts, like CuCl, which gives the *anti* isomers, some porphyrin catalysts are able to reverse the *syn/anti* ratio of the products, depending on the nature of the metal. The mechanism of the metalloporphyrins catalyzed cyclopropanation reactions, was deeply studied but not completely elucidated in all of its aspects, because of both the lability of the bond between the metal, and the acetate residue in the reaction intermediate. [8] Recently, in our laboratory we have been involved in researching the catalytic oxidation of alkenes, the cyclooligomerization of alkynes, and the cyclopropanation of olefins catalyzed by metalloporphyrins [9–11]. This last reaction was extensively investigated, developing iron [12] and rhodium [13] *meso*-tetraphenylporphyrin catalysts used in the homogeneous phase. Recently, we have also reported the immobilization of metalloporphyrins on a Merrifield resin, and their use as catalysts for the cyclooligomerization of alkynes and the cyclopropanation of olefins [14,15]. Several papers have also reported the cyclopropanation reactions of α-substituted styrenes, 1,3-dienes and some terminal alkenes by diazoacetates, catalyzed by metalloporphyrin complexes. [16–20] The choice of the metal, and the possibility of varying both its

electronic properties and the steric hindrance of *meso*-tetraphenylporphyrins—introducing substituents on phenyl groups and/or on β positions of the tetrapyrrolic rings—allows us to modulate both the reaction selectivity, and the stereochemical ratio of the reaction products. The chemical robustness of the rhodium and ruthenium porphyrins, and their high selectivity in cyclopropanation reactions, has encouraged many efforts to obtain the recovery and reusability of these catalysts. The binding of 5,10,15,20-tetraarylporphyrin carbonyl ruthenium complexes to poly(ethyleneglycol), gives a soluble polymer-supported catalyst that can be easily removed from the reaction media—by addition of diethyl ether to the solution or on cooling [19].

In this paper, we report the covalent functionalization and characterization of nanodiamonds (DNDs) with a ruthenium porphyrin, and their usage as catalysts for the cyclopropanation of olefins by EDA.

DNDs have exceptional physiochemical properties and present a broad range of potential applications in nanotechnology research [21–26]. Moreover, this nanomaterial exhibits great potential as a green catalyst in itself, or as catalyst support for a variety of chemical reactions [27]. We also decided to use DNDs in the place of other carbon supports, because the cyclopropanation involves double bonds, this fact giving us side reactions in the unsaturation of the matrix.

The ability of DNDs in these applications are still under investigation, and this research would add value to the field of DNDs porphyrin-based catalysts.

2. Results

The DNDs obtained by the detonation technique are available from commercial sources, but for our purposes, it has been necessary to increase the content of hydroxyl groups on the surface, by a reduction of all of the oxygen containing groups, i.e., ketonic, carboxylic and epoxydic. This was accomplished by a preliminary H_2 plasma treatment by PECVD [28], followed by a chemical reduction by means of a boron hydride reagent under dry conditions, as reported in the literature [23].

Morphological characterization of the plasma reduced DNDs, was performed by transmission electron microscopy (TEM) analysis (Figure 1). The investigation revealed that DNDs are agglutinated in the form of aggregates of several tens of nm, making the study of single particles difficult. Nevertheless, the particles maintain their individuality, so that, by using two different approaches (by taking pictures at different focus values and by the inverse Fourier transform of the HREM pictures diffractogram with one reflection at a time), we were able to measure a remarkable uniformity of the particle size between 5 and 10 nm.
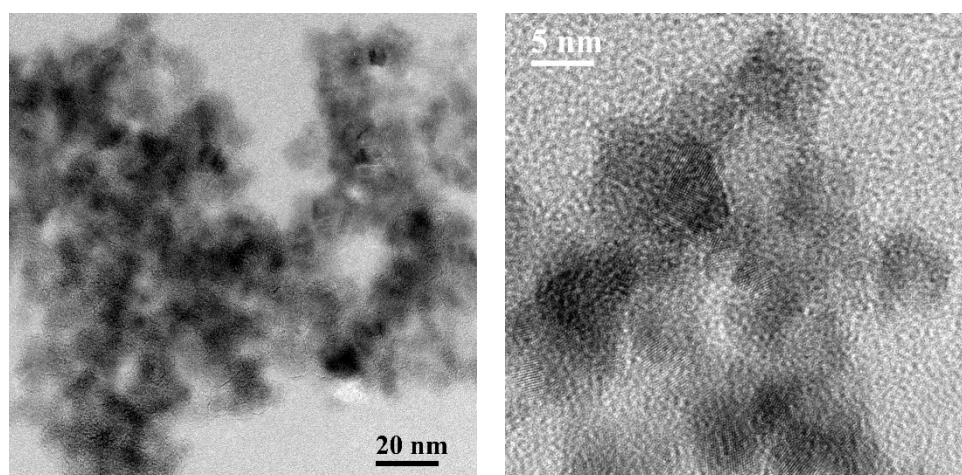

Figure 1. On the left, transmission electron microscopy (TEM) image of plasma treated Detonation nanodiamonds (DNDs); on the right, an enlarged picture at a border of an agglomerate showing some individual particles.

The reduction of the DNDs surface was evaluated by Raman spectroscopy analysis.

Figure 2 reports the spectra of the DNDs sample, as received and after the H_2 plasma treatment. In the Raman spectra of untreated and treated DNDs, the diamond peak is well detectable and located at about 1324 cm^{-1}. The plasma-enhanced chemical vapor deposition (PECVD) treated sample, exhibits an increase in diamond peak intensity, indicating that plasma treatment is effective in eliminating the non-diamond phase.

The broad feature in Raman scattering at 1400–1800 cm^{-1}, can be assigned to the contributions from the sp^3/sp^2 amorphous carbon phase, sp^2 graphitic phase and some surface functional group. The accurate interpretation of the bands occurring in the spatial frequency range, is still under debate in the literature. However, although the Raman spectroscopy appears to not be very sensitive to the surface terminations such as C–H and C–OH, the 1640 cm^{-1} band is commonly attributed to the sp^2 carbon phase [28].
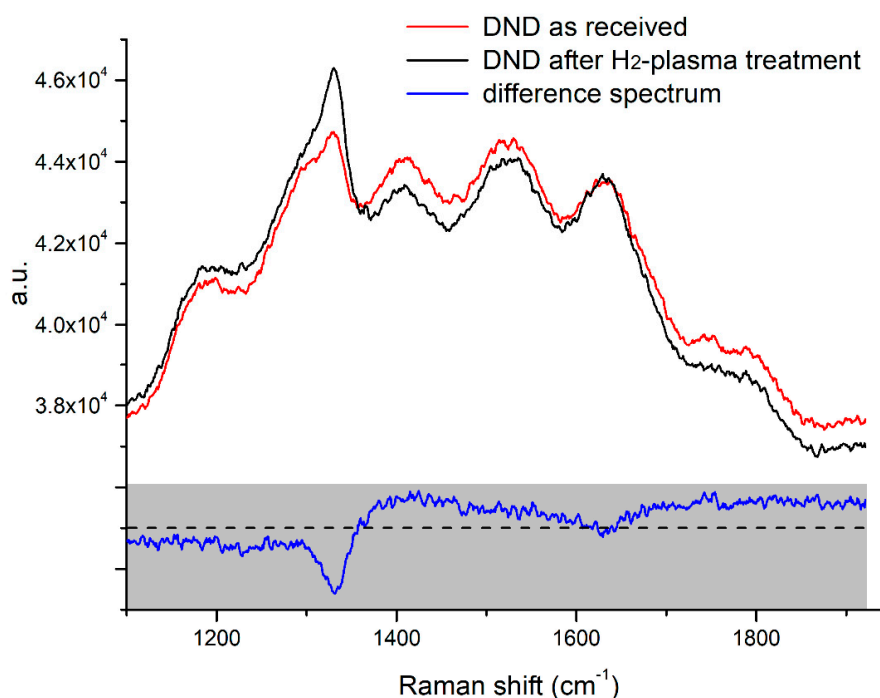

Figure 2. Raman spectra of DNDs sample as received (red line), after the plasma treatment (black line), and the difference spectrum (blue line).

In order to better compare the spectra of treated and untreated sample DNDs, the difference spectrum is reported (as the blue line in Figure 2). The main differences are detected at approximately 1330 cm^{-1}, 1640 cm^{-1} and 1750 cm^{-1}, indicating that the treatment is effective in reducing sp^2 phase. The fact that the shoulder signals at approximately 1750 cm^{-1}, could be related to the C=O bonds located on the DNDs surface. The decreasing of these bands for the treated DNDs, could indicate a reduction of this oxygenated functional group on the DND surface, after the plasma treatment [29].

The plasma treated and subsequently chemically reduced DNDs, were functionalized by the use of (3-aminopropyl)trimethoxysilane, as reported in Scheme 1 [30].
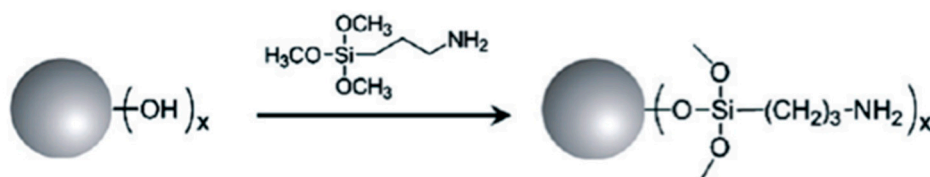
Scheme 1. Silanization of the DNDs.

The functionalization with Ru-TF$_5$-tetraphenylporphyrin, has been obtained using the well-known nucleophilic aromatic substitution of the activated fluorine atom of the phenyl rings, by the amine group of the silane, as reported in Scheme 2 [31].
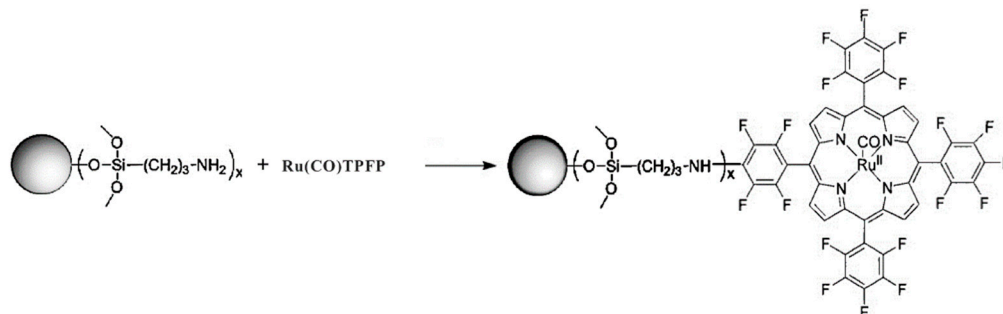
Scheme 2. Functionalization of the DNDs.

The functionalization of the DNDs was checked by the X-ray photoelectron spectroscopy (XPS). The measurements were carried out on the silanized nanodiamonds functionalized with the metalloporphyrin, in order to investigate the resulting chemical composition and the covalent binding of the silane, and consequently of the Ru-porphyrin, on the surface of the DNDs. XPS allows us to effectively distinguish the porphyrins from porphyrinate. The XPS analysis performed on the functionalized DNDs ruthenium porphyrin catalyst showed a unique N 1s peak in the imino-pyrrolic region, typical of the porphyrinate nitrogens (399 eV). This is, therefore, diagnostic of the presence of a porphyrin and, thus, of the successful coordination of ruthenium in the porphyrin core, demonstrating its presence on the surface of the nanodiamonds. The sample also has a clear additional component, probably due to the amino group of the linker (3-aminopropyltriethoxysilane), which is found in the ratio 1:4 with the peak of nitrogen from the porphyrinate, confirming its anchoring bond to the hydroxylated nanodiamonds. However, the peak of Ru 3d (which is located very close to the peak of C 1s) was not detected, because it reasonably represents a minimum percentage with respect to the large quantity of carbon in the nanodiamond.

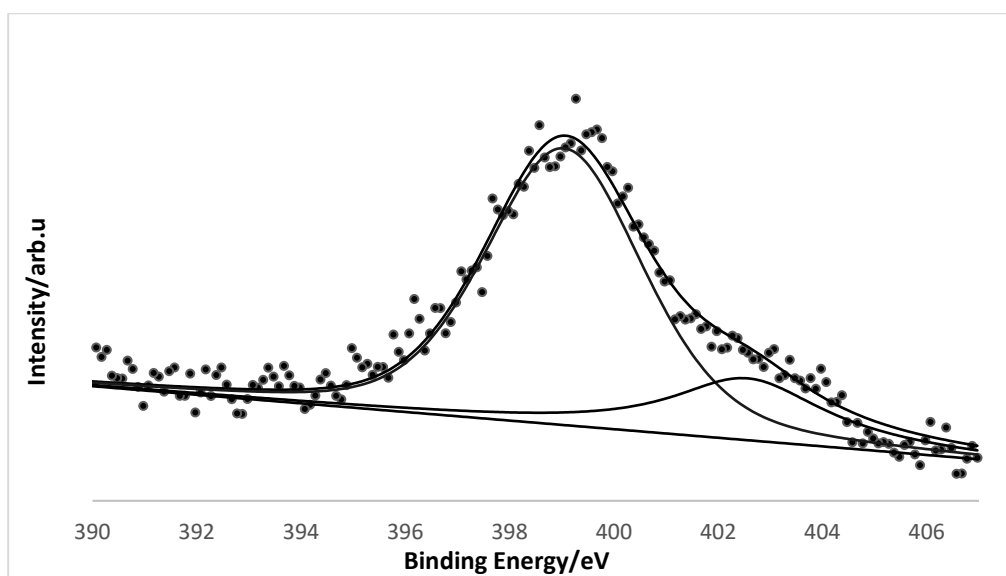In Figure 3, the XPS spectrum of the N 1s peak is reported.

Figure 3. N 1s peak of the metalloporphyrin functionalized DNs.

The analysis of the morphology of the functionalized DNDs, was performed by a local analysis at the nanoscale, by means of the HAADF-STEM technique. Under proper conditions, the contrast intensity of the images is highly sensitive to variations of the atomic number of the elements in the sample under investigation. In Figure 4a, a typical high-angle annular dark field (HAADF) image of the sample is reported, and we can observe the sample appear as approximately 200 nm sized aggregates, given by a high density of homogenously distributed DNDs particles. Figure 4b reports the electron diffraction pattern of the same aggregate, showing the peculiar diffraction signals of the polycrystalline diamond. Specifically, the rings relating to reflections from the (111) (d = 0.206 nm), (220) (d = 0.126 nm) and (311) (d = 0.107 nm) planes, are evident in the picture.
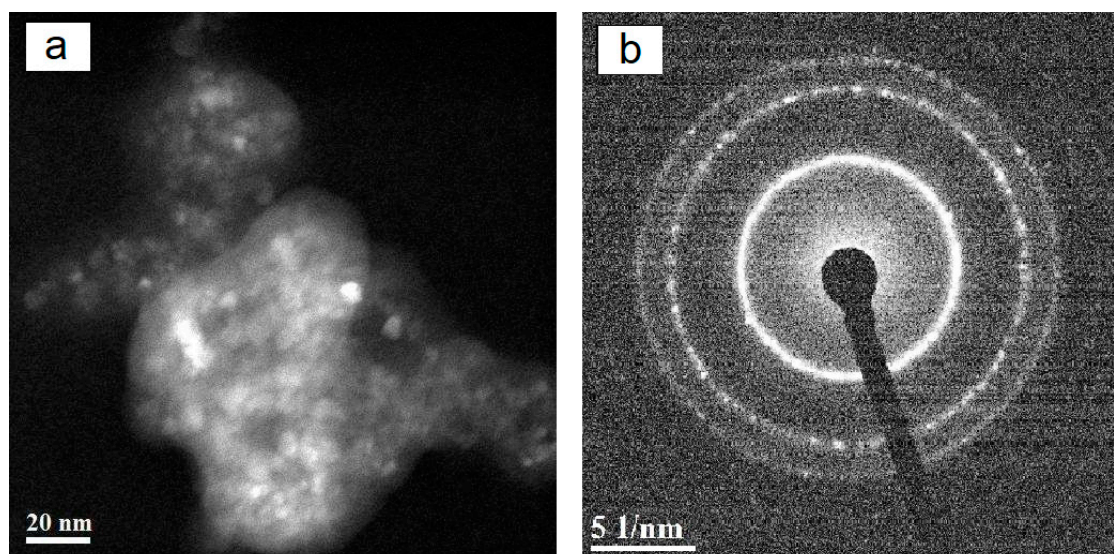

Figure 4. Morphological and structural characterizations of a functionalized DNDs aggregate: (**a**) scanning TEM high-angle annular dark field (HAADF) image, (**b**) selected area diffraction (SAED) pattern.

3. Discussion

Our heterogeneous catalyst was tested in the cyclopropanation reaction, with different olefins such as styrene, 4-methoxystyrene, 4-chlorostyrene, norbornene, 1-methylcyclopentene and 2,2,4-trimethylpentene. All of the reactions were carried out under the same conditions, with ethyldiazoacetate (EDA) and the olefin dissolved in dry CHCl$_3$, following the standard procedure as described in the experimental section. At the end of the reaction, an internal standard was added, and the reaction products were analyzed by gas chromatography (GC). The data resulting from the reactions are reported in Table 1.

Table 1. Results for the cyclopropanation of olefins catalyzed by Ru-porphyrin functionalized DNDs. The yields were calculated from the EDA.

Entry	Substrate	Yield%	Syn/Anti Ratio
1	Styrene	35 (60 [a])	1:2.5 (1:0.9 [a])
2	4-Cl-Styrene	25 (55 [a])	1:3.8 (1:0.9 [a])
3	4-OCH$_3$-Styrene	34 (59 [a])	1:3.2 (1:0.55 [a])
4	Norbornene	38 (51 [a])	1:20 (1:0.8 [a])
5	1-methylcyclopentene	- (45 [a])	-
6	2,4,4-trimethylpentene	- (70 [a])	-

[a] From ref. [14] with rhodium porphyrin-Merrifield resin adduct.

We also performed some further control experiments using non functionalized DNs. These experiments did not give any cyclopropanation products, giving us further proof of the functionalization of the nanodiamonds.

The yields and the *syn/anti* ratios for styrene, 4-chlorostyrene and 4-methoxystyrene appear basically comparable, demonstrating how the electronic nature of the substituent on the phenyl has a low effect. Since the catalyst consists of a great concentration of fluorine atoms, we think that, during the catalytic reaction, aromatic olefins can approach the core of the macrocycle through a π–π interaction with the fluorinated rings, stabilizing the transition state which leads to the *anti* isomer [3]. On the other hand, no cyclopropane formation was observed in the reactions performed on aliphatic olefins 1-methylcyclopentene and 2,4,4-trimethylpentene, even when varying the reaction conditions. In our opinion, this is probably due to a different carbene transfer mechanism from the metal to the double bond of the substrate. The excellent *anti*-selectivity observed with norbornene is noteworthy. The presence of sterical hindrance in the catalytic sites, probably affects the products' distribution. The lower yields of the reactions compared with those reported in a previous investigation [14], could be due to the minor amount of ruthenium porphyrin molecules bound onto the nanodiamonds surface.

4. Materials and Methods

4.1. General

The UV-vis spectra were recorded with a Varian Cary 10 spectrophotometer (Varian, Australia) and ^{1}H NMR spectra were recorded on a Bruker AM 400 spectrometer (Karlsruhe, Germany) as CDCl$_3$ solutions. Chemical shifts are given in ppm from tetramethylsilane (TMS) and are referenced against residual solvent signals. Mass spectra (FAB) were recorded on a VG-Quattro spectrometer (Manchester, UK), using 3-nitrobenzyl-alcohol (NBA) as a matrix. The FT-IR spectra were routinely recorded on a Perkin Elmer Spectrum One spectrometer (Waltham, MA, USA), and XPS spectra were obtained on a modified Omicron NanoTechnology MXPS system (GmbH Taunusstein, Germany). TEM studies were carried out within a JEOL 2200FS (Akishima, Tokyo, Japan) field emission microscope operating at 200 kV, with a point-to-point resolution of 0.185 nm, equipped with an in-column Ω filter, an X-ray microanalysis, and two HAADF detectors, for chemical imaging. DNDs powders dispersed in chloroform, and treated with ultrasounds for 15 min were deposited on carbon grids for the analysis. Raman Spectroscopy was performed with a Horiba micro-Raman spectrometer XploRA ONE^{TM} (HORIBA, Ltd, Hakata Fukoku Building, Tenyamachi, Hakata-ku Fukuoka, Japan), equipped with a 532 nm laser. Excitation spectra were recorded and analyzed in the 1000–2000 cm^{-1} wavenumber region.

The products' yields, and the isomeric ratios for all of the reactions, were measured by GC analyses, with a Focus Thermo Fisher Instrument (Waltham, MA, USA), using helium as the carrier gas (35 cm/s). A fused silica Supelco capillary columns SPB-5 (30 m × 0.25 mm i.d.; 0.25 mm film thickness), was used. The gas chromatographic conditions were as follows: initial temperature, 70 °C for 1 min; temperature increase rate, 20 °C/min; final temperature, 200 °C; injector temperature, 150 °C; detector temperature, 230 °C.

The chemical yields were determined by adding a suitable internal standard (decane or dodecane) to the reaction mixture at the end of each experiment and were reproducible within ±2% for multiple experiments. The analytical data for cyclopropane derivatives of styrene, 4-chlorostyrene, 4-methoxystyrene and norbornene are reported in the literature [14].

4.2. Chemicals

All of the reagents and solvents (Aldrich Chemical, Merck KGaA, Darmstadt, Germany), were of the highest analytical grade, and were used without further purification. The silica gel 60 (70–230 and 230–400 mesh, Merck KGaA, Darmstadt, Germany), was used for column chromatography. High-purity

grade nitrogen gas was purchased from Rivoira. The free base H_2-TF_5-tetraphenylporphyrin, was purchased from Aldrich.

The nanodiamonds used for this work were purchased from Altai Technical State University, Barnaul, Russian Federation.

The ruthenium TF_5-tetraphenylporphyrin carbonyl was obtained as reported in the literature [32] and was compared with a commercially available sample from Porphyrin Products.

4.3. Synthesis

4.3.1. Reduction of DNDs

DNDs powders were subjected to a hydrogen plasma-assisted CVD treatment, to remove the non-diamond carbon and reduce the oxygen species at the NDs surface.

The process was carried out by using a custom designed Plasma Enhanced Chemical Vapour Deposition (PE-CVD) reactor, where the gas phase was excited by a dual-mode MW/RF plasma [28]. The parameters adopted for the reduction experiment were the MW and RF powers at 100 W, a H_2 flux of 100 sccm, and a reduction time of 10 min. The sample temperature was fixed at $550 \pm 10\,^{\circ}$C.

Five hundred milligrams of the CVD-treated DNDs was then suspended in 30 mL of dry THF, and 5 mL of 1 M BH_3 THF was added dropwise under the nitrogen. Following this, the mixture was refluxed for 24 h, and after cooling to room temperature, the diluted HCl was added until the hydrogen evolution ended. The obtained solid product was isolated by centrifugation, and then subjected to water washing and centrifugation cycles, until the supernatant liquid presented a neutral pH. The sample, after drying in a vacuum, appeared as a grey powder (400 mg).

4.3.2. Covalent Functionalization of DNDs with (3-Aminopropyl)Trimethoxysilane (APS)

Two hundred and twenty-five milligrams of reduced DNDs was added to 31.5 mL of a 5% solution of APS, and stirred for 48 h at 60 °C. The sample was isolated by centrifugation, and then washed with 10 mL of acetone and isolated by centrifugation yielding 186 mg of a grey powder, after drying in a vacuum.

4.3.3. Functionalization of NDs with Ru(TF_5PP)CO

One hundred and twenty milligrams of silanized DNDs in 30 mL of toluene, was added to 42 mg of Ru-TF_5-tetraphenylporphyrin carbonyl. The mixture was stirred at 120 °C for 4 h. After centrifugation, the precipitate was subjected to 3 consecutive washing/centrifugation cycles with 10 mL of chloroform each, and finally dried in a vacuum, yielding 108 mg of a brownish powder.

4.4. Typical Cyclopropanation Reactions

Zero-point-two milliliters (1.9 mmol) of ethyldiazoacetate and 0.7 mL (6.64 mmol) of styrene, were dissolved in 3 mL of dry $CHCl_3$. Then, 10 mg of DNDs catalyst were added, and the resulting solution was refluxed for 12 h. At the end of the reaction, decane was added as an internal standard, and the mixture was analyzed by GC (Focus Thermo Fisher Instrument, Waltham, MA, USA).

4.5. Recycling of the Catalyst

At the end of the reaction, the solvent was evaporated under vacuum, and the solid was washed with three portions of fresh chloroform, each time using centrifugation to obtain the solid. The solution remained clear and the UV-vis analysis showed the absence of any free catalyst in the solution. The catalyst was dried under vacuum and reused for a new reaction. The yield of the reaction did not change under the experimental conditions, after four recyclings and within the experimental error.

5. Conclusions

In this paper, we showed the possibility for the covalent functionalization of DNDs with a metalloporphyrin, and the potential use of this adduct for catalyzing the cyclopropanation reaction of olefins. The catalyst can be recovered by a simple centrifugation and can be reused several times without losing its activity. This functionalization, and the use of the DNDs, opens up new fields of research for these new materials, which can be used in several applications.

References

1. Pogacic, V.; Bullock, A.N.; Federov, O.; Filippakopoulos, P.; Gasser, C.; Biondi, A.; Meyer-Monard, S.; Knapp, S.; Schwaller, J. Structural Analysis Identifies Imidazo [1,2-b]Pyridazines as PIM Kinase Inhibitors with In vitro Antileukemic. *Activity Cancer Res.* **2007**, *67*, 6916–6924. [CrossRef] [PubMed]

2. Doyle, M.P. Catalytic methods for metal carbene transformations. *Chem. Rev.* **1986**, *86*, 919–939. [CrossRef]

3. Robbins Wolf, J.; Hamaker, C.G.; Djukic, J.-P.; Kodadek, T.; Woo, L.K. Shape and stereoselective cyclopropanation of alkenes catalyzed by iron porphyrins. *J. Am. Chem. Soc.* **1995**, *117*, 9194–9199. [CrossRef]

4. Maxwell, J.L.; Brown, K.C.; Bartley, D.W.; Kodadek, T. Mechanism of the Rhodium Porphyrin-Catalyzed Cyclopropanation of Alkenes. *Science* **1992**, *256*, 1544–1547. [CrossRef] [PubMed]

5. Hamaker, C.G.; Djukic, J.-P.; Smith, D.A.; Woo, L.K. Mechanism of Cyclopropanation Reactions Mediated by 5,10,15,20-tetra-(p-tolylporphyrinato)osmium(II) Complexes. *Organometallics* **2001**, *20*, 5189–5199. [CrossRef]

6. Penoni, A.; Wanke, R.; Tollari, S.; Gallo, E.; Musella, D.; Ragaini, F.; Demartin, F.; Cenini, S. Cyclopropanation of Olefins with Diazoalkanes, Catalyzed by CoII(porphyrin) Complexes—A Synthetic and Mechanistic Investigation and the Molecular Structure of CoIII(TPP)(CH$_2$CO$_2$Et) (TPP = Dianion of *meso*-Tetraphenylporphyrin). *Eur. J. Inorg. Chem.* **2003**, *2003*, 1452–1460. [CrossRef]

7. Galardon, E.; Le Maux, P.; Simonneaux, G. Cyclopropanation of Alkenes with Ethyldiazoacetate Catalysed by Ruthenium Porphyrin Complexes. *Chem. Comm.* **1997**, 927–928. [CrossRef]

8. Callot, H.J.; Metz, E.; Piechocki, C. Sterically crowded cyclopropanation catalysts. Syn-selectivity using rhodium(III)porphyrins. *Tetrahedron* **1982**, *38*, 2365–2369. [CrossRef]

9. Baciocchi, E.; Boschi, T.; Cassioli, L.; Galli, C.; Jaquinod, L.; Lapi, A.; Paolesse, R.; Smith, K.M.; Tagliatesta, P. Electronic Effects on the Stereoselectivity of Epoxidation Reactions Catalyzed by Manganese Porphyrins. *Eur. J. Org. Chem.* **1999**, *1999*, 3281–3286. [CrossRef]

10. Crestini, C.; Pastorini, A.; Tagliatesta, P. The Immobilized Porphyrin-Mediator System Mn(TMePyP)/clay/HBT(clay-PMS): A Lignin Peroxidase Biomimetic Catalyst in the Oxidation of Lignin and Lignin Model Compounds. *J. Mol. Catal. A Chem.* **2004**, *208*, 195–202. [CrossRef]

11. Conte, V.; Elakkari, E.; Floris, B.; Mirruzzo, V.; Tagliatesta, P. The Cyclooligomerization of Arylethynes in Ionic Liquids Catalysed by Ruthenium Porphyrins: A Case of Real Catalyst Recycling. *Chem. Commun.* **2005**, 1587–1588. [CrossRef] [PubMed]

12. Tagliatesta, P.; Pastorini, A. Remarkable Selectivity in the Cyclopropanation Reactions Catalysed by an Halogenated Iron *meso*-Tetraphenylporphyrin. *J. Mol. Catal. A Chem.* **2003**, *198*, 57–61. [CrossRef]

13. Tagliatesta, P.; Pastorini, A. Electronic and Steric Effects on the Stereoselectivity of Cyclopropanation Reactions Catalyzed by Rhodium *meso*-Tetraphenylporphyrins. *J. Mol. Catal. A Chem.* **2002**, *185*, 127–133. [CrossRef]

14. Ciammaichella, A.; Leoni, A.; Tagliatesta, P. Ruthenium porphyrin bound to a Merrifield resin as heterogeneous catalyst for the cyclooligomerization of arylethynes. *New J. Chem.* **2010**, *34*, 2122–2124. [CrossRef]

15. Ciammaichella, A.; Cardoni, V.; Leoni, A.; Tagliatesta, P. Rhodium Porphyrin Bound to a Merrifield Resin as Heterogeneous Catalyst for the Cyclopropanation Reaction of Olefins. *Molecules* **2016**, *21*, 278. [CrossRef]

16. Chen, Y.; Ruppel, J.V.; Zhang, X.P.J. Cobalt-Catalyzed Asymmetric Cyclopropanation of Electron-Deficient Olefins. *J. Am. Chem. Soc.* **2007**, *129*, 12074–12075. [CrossRef]

17. Anding, B.J.; Ellern, A.; Woo, L.K. Olefin Cyclopropanation Catalyzed by Iridium (III) Porphyrin Complexes. *Organometallics* **2012**, *31*, 3628–3635. [CrossRef]

18. Xu, X.; Zhu, S.; Cui, X.; Wojtas, L.; Zhang, X.P. Cobalt (II)-Catalyzed Asymmetric Olefin Cyclopropanation with α-Ketodiazoacetates. *Angew. Chem. Int. Ed.* **2013**, *52*, 11857–11861. [CrossRef]

19. Otte, M.; Kuijpers, P.F.; Troeppner, O.; Ivanovic-Burmazovic, I.; Reek, J.N.H.; de Bruin, B. Encapsulated Cobalt-Porphyrin as a Catalyst for Size-Selective Radical-type Cyclopropanation Reactions. *Chem. Eur. J.* **2014**, *20*, 4880–4884. [CrossRef]

20. Dzik, W.I.; Xu, X.; Zhang, X.P.; Reek, J.N.H.; de Bruin, B. 'Carbene Radicals' in CoII(por)-Catalyzed Olefin Cyclopropanation. *J. Am. Chem. Soc.* **2010**, *132*, 10891–10902. [CrossRef]

21. Mochalin, V.N.; Shenderova, O.; Ho, D.; Gogotsi, Y. The properties and applications of nanodiamonds. *Nat. Nanotech.* **2012**, *7*, 11–23. [CrossRef] [PubMed]

22. Baidakova, M.; Vul, A. New prospects and frontiers of nanodiamond clusters. *J. Phys. D Appl. Phys.* **2007**, *40*, 6300–6311. [CrossRef]

23. Tamburri, E.; Guglielmotti, V.; Orlanducci, S.; Terranova, M.L.; Sordi, D.; Passeri, D.; Matassa, R.; Rossi, M. Nanodiamond-mediated crystallization in fibers of PANI nanocomposites produced by template-free polymerization: Conductive and thermal properties of the fibrillar networks. *Polymer* **2012**, *53*, 4045–4053. [CrossRef]

24. Tamburri, E.; Guglielmotti, V.; Matassa, R.; Orlanducci, S.; Gay, S.; Reina, G.; Terranova, M.L.; Passeri, D.; Rossi, M. Detonation nanodiamonds tailor the structural order of PEDOT chains in conductive coating layers of hybrid nanoparticles. *J. Mater. Chem. C* **2014**, *2*, 3703–3716. [CrossRef]

25. Reina, G.; Orlanducci, S.; Cairone, C.; Tamburri, E.; Lenti, S.; Cianchetta, I.; Rossi, M.; Terranova, M.L. Rhodamine/nanodiamond as a system model for drug carrier. *J. Nanosci. Nanotechnol.* **2015**, *15*, 1022–1029. [CrossRef] [PubMed]

26. Orlanducci, S. Gold-Decorated Nanodiamonds: Powerful Multifunctional Materials for Sensing, Imaging, Diagnostics, and Therapy. *Eur. J. Inorg. Chem.* **2018**, *48*, 5138–5145. [CrossRef]

27. Arnault, J.-C. (Ed.) *Nanodiamonds: Advanced Material Analysis, Properties and Applications*; Nanodiamonds for Catalytic Reactions; Elsevier: Amsterdam, The Netherlands, 2017; Chapter 18.

28. Toschi, F.; Orlanducci, S.; Guglielmotti, V.; Cianchetta, I.; Magni, C.; Terranova, M.L.; Pasquali, M.; Tamburri, E.; Matassa, R.; Rossi, M. Hybrid C-nanotubes/Si 3D nanostructures by one-step growth in a dual-plasma reactor. *Chem. Phys. Lett.* **2012**, *539*, 94–101. [CrossRef]

29. Mermouxa, M.; Chang, S.; Girard, H.A.; Arnault, J.-C. Raman spectroscopy study of detonation nanodiamond. *Diam. Relat. Mater.* **2018**, *87*, 248–260. [CrossRef]

30. Krueger, A.; Liang, Y.; Jarre, G.; Stegk, J. Surface Functionalisation of Detonation Diamond Suitable for Biological Applications. *J. Mater. Chem.* **2006**, *16*, 2322–2328. [CrossRef]

31. Kadish, K.M.; Han, B.C.; Franzen, M.M.; Araullo-McAdams, C. Syntheses and spectroscopic characterization of (T(p-Me2N)F$_4$PP)H$_2$ and (T(p-Me$_2$N)F$_4$PP)M where T(p-Me$_2$N)F$_4$PP = the dianion of *meso*-tetrakis(o,o,m,m-tetrafluoro-p- (dimethylamino)phenyl)porphyrin and M = cobalt(II), copper(II), or nickel(II). Structures of (T(p-Me$_2$N)F$_4$PP)Co and meso-tetrakis(pentafluorophenyl) porphinatocobalt(II), (TF$_5$PP)Co. *J. Am. Chem. Soc.* **1990**, *112*, 8364–8368.

32. Kadish, K.M.; Hu, Y.; Tagliatesta, P.; Boschi, T. Synthesis and electrochemical characterization of ruthenium porphyrins containing a bound PF$_3$ axial ligand. *J. Chem. Soc. Dalton Trans.* **1993**, 1167–1172. [CrossRef]